Clear evidence of interfacial anomalous Hall effect in epitaxial $L1_0$ FePt and FePd films

Shi-Jie Xu, Zhong Shi,* and Shi-Ming Zhou†

Shanghai Key Laboratory of Special Artificial Microstructure and Pohl Institute of Solid State Physics and School of Physics Science and Engineering, Tongji University, Shanghai 200092, China

(Received 15 March 2018; published 16 July 2018)

Anomalous Hall effect in epitaxially grown $L1_0$-ordered FePd and FePt films on MgO(001) has been investigated as a function of the film thickness (d). It is found that the anomalous Hall resistivity can be described by conventional scaling law, i.e., $\rho_{AH} = a\rho_{xx} + b\rho_{xx}^2$ with longitudinal resistivity ρ_{xx}. It is interesting to find that both a and b parameters approximately change as a linear function of the inverse film thickness. The linear $1/d$ dependencies can be attributed to the symmetry breaking at the surface. Moreover, the bulk and in particular the surface contributions to the parameters a and b in $L1_0$ FePt films are enhanced, compared with those of $L1_0$ FePd films, due to larger spin orbit interaction of heavier Pt atoms. It is indicated that not only the bulk but also the interface components of a and b are tuned by the spin-orbit interaction. The present results might stimulate further theoretical investigation of the mechanism of the anomalous Hall effect.

DOI: 10.1103/PhysRevB.98.024413

I. INTRODUCTION

Spintronic devices, as an alternative to electronics, utilize both charge and spin properties of electrons. The three central research themes in spintronics are generation, manipulation, and detection of pure spin current, for which the spin-orbit coupling plays an important role by means of the spin Hall effect (SHE) [1,2]. Very recently, it is demonstrated the interface contribution, along with the bulk effect, can largely affect the SHE [3–6]. Anomalous Hall effect (AHE), discovered by Edwin Hall in 1881 in ferromagnets [7], has received intensive renewed interest in the past few years because of its similar mechanism to SHE [8]. The anomalous Hall resistivity in ferromagnetic materials, ρ_{AH}, is described by the empirical scaling law $\rho_{AH} = a\rho_{xx} + b\rho_{xx}^2$, where ρ_{xx} is the longitudinal resistivity [8]. For the intrinsic mechanism based on the Berry phase of Bloch states, the dependence of $\rho_{AH} \propto \rho_{xx}^2$ follows [9], whereas for the extrinsic skew scattering and the side-jump, ρ_{AH}, is expected to proportional to ρ_{xx} and ρ_{xx}^2, respectively [10–12].

Magnetic metal films are born to be natural object for the investigation of AHE [13–19]. In most studies of the AHE scaling law [13–16], the interfacial resistivity and the bulk one are often equally treated and the interfacial effect has not been clearly addressed although the anomalous Hall resistivity and the sheet resistivity both change with the film thickness when the film thickness is comparable with or smaller than the mean free path of electrons [20–23]. In particular, the values of anomalous Hall conductivity (AHC) in $L1_0$ FePt films reported by various research groups are different [24–29]. The inconsistency is attributed to either different film thickness or chemical ordering degree or both of them. Therefore, effects of electron scattering at surface/interface should be separated from the bulk one.

In this work, AHE in high-quality epitaxially grown $L1_0$ FePt and FePd ordered alloy films is studied as a function of the film thickness (d). It is found that AHE for $L1_0$ FePd and FePt alloys films can be well described by the conventional scaling law. The linear parameter a and the quadratic parameter b can both be fitted with the linear function of $1/d$. The surface effect plays a significant role for thin films and can be ignored with the dominant bulk contribution when the film is thicker than 20.0 nm. The symmetry-breaking effect is clearly demonstrated on the AHE.

II. EXPERIMENTS

Two series of $L1_0$ FePt and FePd alloy films with different film thicknesses were deposited on MgO(001) single crystal substrates by dc magnetron sputtering. The base pressure was 3.0×10^{-5} Pa and Ar pressure was 0.5 Pa during deposition. FePt and FePd composite targets were formed by putting small Pt or Pd pellets onto the Fe target. The deposition rate of FePt and FePd was about 0.15 nm/s. The substrate was kept at an elevated temperature in the region of 620 °C–700 °C. After deposition, the samples were post-annealed at the same substrate temperature for 2 h. The substrate temperature was at 620 °C for thin films and was enhanced for thick ones to guarantee high quality of all epitaxial ordered samples with different film thicknesses. The microstructure was characterized by x-ray diffraction (XRD) by a Bruker D8 diffractometer with a five-axis configuration and Cu Kα ($\lambda = 0.1542$ nm). The film thickness and the surface roughness were characterized by x-ray reflectivity (XRR) and atomic force microscope (AFM). The epitaxial growth of films was proven by the x-ray pole figures. The alloy composition was measured by energy dispersive x-ray spectroscopy. Hysteresis loops and spontaneous magnetization M_S as a function of temperature (T) were measured by physical property measurement system (Quantum Design PPMS-9 T system). The longitudinal resistivity ρ_{xx} and

*shizhong@tongji.edu.cn
†shiming@tongji.edu.cn

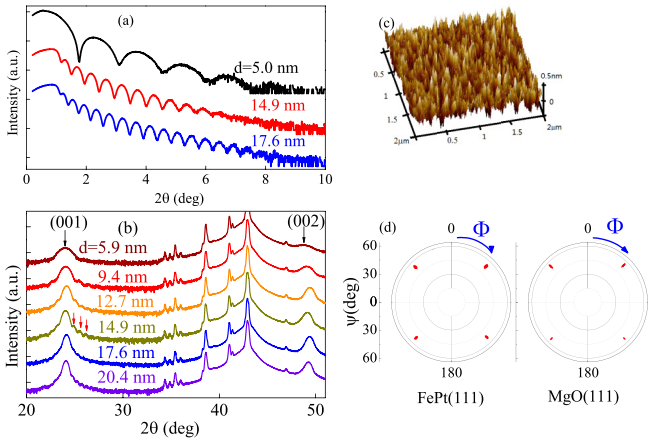

FIG. 1. XRR (a) and XRD patterns (b) of epitaxial FePt films with different thickness, atomic force microscope pattern of 17.6-nm-thick FePt film (c), and pole figures of 17.6-nm-thick FePt film ($2\theta = 41.05^\circ$) and the corresponding MgO substrates ($2\theta = 36.94^\circ$) (d). For clarification, the curves in (a) and (b) are vertically shifted. The small red arrows in (b) mark the Laue oscillations of the 14.9-nm-thick sample.

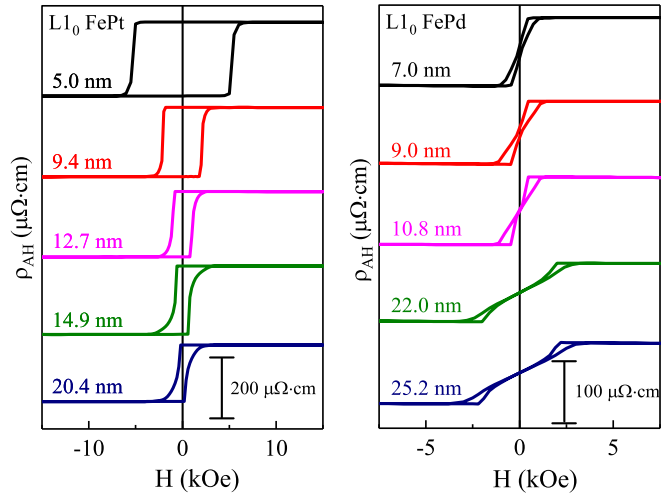

FIG. 2. Measured Hall loops of $L1_0$ FePt (left column) and FePd (right column) films. The inset numbers refer to film thickness. The measurements were performed at 275 K. For FePt films, the curves are offset by 1030, 760, 490, 240, and 0 $\mu\Omega$ cm for $d = 5.0$, 9.4, 12.7, 14.9, and 20.4 nm, respectively. The curves of FePd are shifted by 400, 300, 200, 100, and 0 $\mu\Omega$ cm for $d = 7.0$-, 9.0-, 10.8-, 22.0-, and 25.2-nm films, respectively.

transverse resistivity ρ_{xy} were measured in the temperature region from 5 K to 300 K with standard Hall bar patterns. The anomalous Hall resistivity ρ_{AH} was obtained by extrapolation from the high to zero magnetic fields [30].

III. RESULTS AND DISCUSSION

Figures 1 (a) and 1(b) present typical XRR and XRD spectra of the $L1_0$ FePt films, respectively. Kiessig fringes of all FePt films are observed in a wide angular region. By fitting the reflected amplitude of the x ray, the film surface roughness, as the standard deviation of the Fresnel coefficient, is fitted to be in the region of 0.3–0.7 nm, mainly following the surface roughness of MgO substrates. A typical AFM image for the 17.6-nm-thick $L1_0$ FePt is shown in Fig. 1(c). The AFM roughness of all samples is less than 0.6 nm, in agreement with the XRR results. For FePt films on MgO(001), two diffraction peaks near $2\theta = 24^\circ$ and 49° correspond to FePt(001) and FePt (002) orientations, respectively, as shown in Fig. 1(b). For FePt films thicker than 5.9 nm, Laue oscillations occur near the (001) superlattice diffraction peak, indicating large coherent length and better film quality for thick samples. For the thinnest sample investigated here ($d = 5.9$ nm), however, the Laue fringes are hidden in the background near the wide (001) XRD peak, in spite of low surface roughness. This phenomenon may be caused by either the broadening of the (001) peak due to smaller crystalline grains or by the suppression of Laue oscillations due to few coherently scattering lattice planes. For thick samples, the film thickness can be also fitted from the Laue oscillation near (001) peak. The angular position θ_n of the nth Laue oscillation peak can be obtained by following equation [31], $2\sin\theta_n/\lambda = 1/d_{001} + n/d$, where λ, d_{001}, and d are the wavelength of the x ray, the interplane atomic distance along the film normal direction, and the film thickness, respectively. For example, the value of d is fitted to be 14.6 nm from Laue oscillation and 14.9 nm from Kiessig fringes. The diffraction peak around $2\theta = 24^\circ$ indicates the establishment of the long-range chemical ordering. The ordering degree in $L1_0$ FePt films is calculated by the following equation, $S = 0.85 \times \sqrt{I(001)/I(002)}$ with the integrated intensities $I(001)$ and $I(002)$ [31–33]. Since peak positions of FePt(002) and MgO(002) are close to each other, the FePt(002) peak intensity is obtained by subtracting the MgO(002) intensity as assuming the Lorentz shape of MgO(002). The ordering parameter of all samples, $S = 0.90 \pm 0.10$, increases slightly with the film thickness. For 20.4-nm and 5.9-nm $L1_0$ FePt samples, for instance, the $I(001)/I(002)$ ratio is 1.35 and 1.07 and the chemical ordering is 0.95 and 0.88, respectively. Moreover, the lattice constant along the film normal direction can be determined by the diffraction spectrum of (001) plane and then the in-plane ones were determined by the off-axis diffraction spectra of (111) and (110) planes. For $d = 20.4$ nm, for example, the lattice constant along the film normal direction and the in-plane ones are 0.367 nm and 0.389 nm, respectively. Finally, the epitaxial growth of the FePt films is confirmed by pole figures of Φ and Ψ scan with fixed 2θ for the (111) orientation. Typical pole figures of FePt and MgO substrate are shown in Fig. 1(d). The poles at $\Phi = 45^\circ$, 135°, 225°, and 315° degrees represent the fourfold symmetry and epitaxial growth of FePt on MgO(001). High-quality epitaxially grown $L1_0$ FePd films are also confirmed after similar microstructural characterization.

The films were then patterned into standard Hall bar. Hall loops of $L1_0$-ordered FePt and FePd with different thicknesses are obtained from dc electric measurements in PPMS. Figures 2(a) and 2(b) show that the Hall loops, at 275 K, are squared for $L1_0$-ordered FePt films and slanted for $L1_0$-ordered FePd films, indicating high and low perpendicular magnetic anisotropy in the former and the latter systems, respectively. For $L1_0$ FePd films with the vortexlike hysteresis

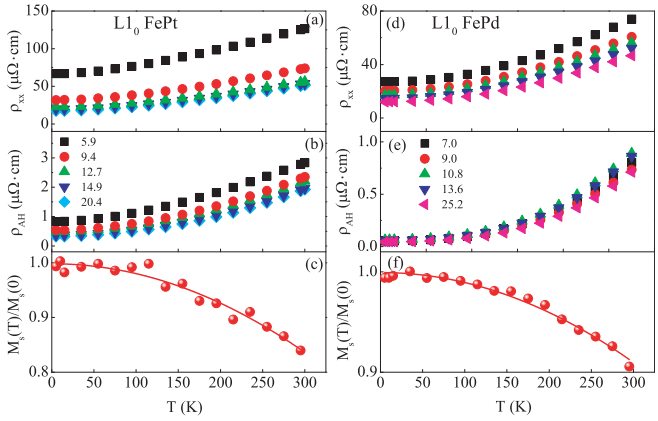

FIG. 3. [(a) and (d)] ρ_{xx}, [(b) and (e)] ρ_{AH}, and [(c) and (f)] normalized spontaneous magnetization M_S for $L1_0$ FePt [(a)–(c)] and FePd [(d)–(f)]. The inset numbers in (a), (b), (d), and (e) refer to film thickness in the unit of nanometers. In (c) and (f), the film thickness is 17.6 and 22.0 nm, respectively. Solid lines in (c) and (f) refer to the T^2 fitting results.

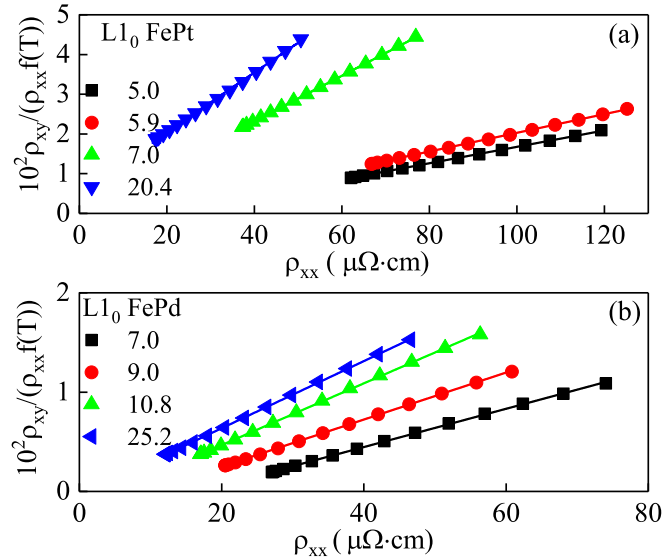

FIG. 4. $\rho_{\mathrm{AH}}/[\rho_{xx}f(T)]$ versus ρ_{xx} for $L1_0$ FePt (a) and FePd (b). Solid lines in (a) and (b) refer to a linear fit of $\rho_{\mathrm{AH}}/[\rho_{xx}f(T)] = a_0 + b_0\rho_{xx}$. The inset numbers refer to film thickness in the unit of nanometers.

loops [34,35], the magnetization at zero magnetic field is equal to zero because the perpendicular magnetic anisotropy is overwhelmed by the demagnetization energy. Moreover, for $L1_0$-ordered FePt films, the coercivity becomes larger for thinner samples because the magnetization reversal process is accompanied by the coherent magnetization rotation for thin samples and by multidomain process for thick samples [36]. For all samples, the Hall resistivity is defined as $\rho_{xy} = R_0H + R_HM$, where R_0 and R_H are the ordinary and anomalous Hall coefficients, respectively. The anomalous Hall resistivity ρ_{AH}, is extrapolated at zero magnetic field. It is found that for specific film thickness, $L1_0$ FePt has a larger anomalous Hall resistivity compared to FePd, consistent with the results in Refs. [24,25].

Figure 3 shows that the measured ρ_{xx}, ρ_{AH}, and spontaneous magnetization M_S for $L1_0$ FePt and FePd as a function of temperature (T). The sheet resistivity ρ_{xx} decreases *monotonically* with decreasing T, indicating the vanishing Kondo effect [37], and approaches a constant, obeying Matthiessen's rule [38]. The ρ_{xx} can be fitted by a linear function of T^2, indicating the dominant electron scattering by spin flip [39,40]. For thin samples the resistivity becomes larger, due to the finite-size effect in electrical resistivity of thin metallic films induced by the geometrical limitation of the bulk mean free path of conduction electrons [17]. Figures 3(c) and 3(f) show that M_S decreases with increasing T. For all samples, $M_S(T)$ can be fitted by a linear function of T^2, being due to either the excitation of long wavelength spin waves or the interaction between spin waves or both [41].

Bulk $L1_0$ FePt and $L1_0$ FePd have a Curie temperature T_C of around 740 K [42], thus the measured M_S varies significantly with T due to thermal magnetization fluctuations below room temperature, as shown in Figs. 3(c) and 3(f). *Ab initio* calculations and experimental studies [41,43,44] have shown that the intrinsic AHC and the skew scattering contribution are roughly proportional to $M_S(T)$. The temperature influence can be excluded as done in Refs. [25,26]. Actually, the validity of above assumption is proved by the fact that the $\rho_{\mathrm{AH}}/[\rho_{xx}f(T)]$ ratio for all the samples is a linear function of ρ_{xx} in Fig. 4, where $f(T) = M_S(T)/M_S(0\,\mathrm{K})$. The slope and the intercept of the lines correspond to b_0 (b at 0 K) and a_0 (a at 0 K), respectively. Thicker samples achieve larger anomalous Hall angles, as shown in Fig. 4.

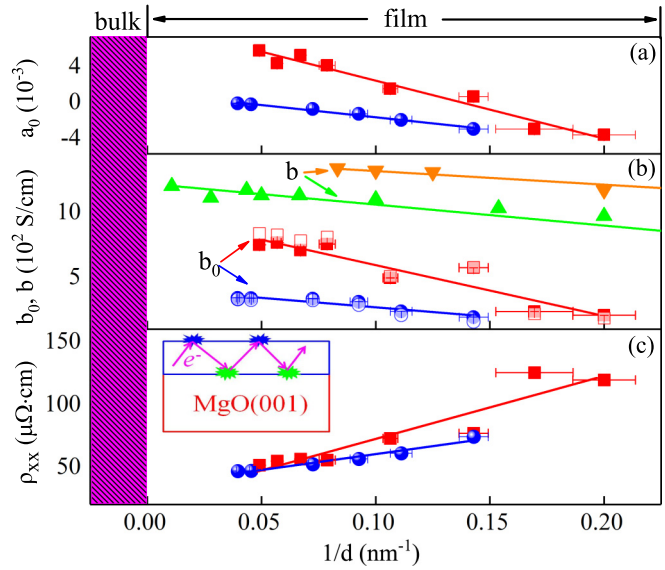

FIG. 5. a_0 (a), b_0 (b), and ρ_{xx} (c) versus $1/d$ for $L1_0$ FePt (solid squares) and FePd (solid circles) films. For comparison, b_0 for $L1_0$ FePt (open squares) and FePd (open circles), and b for epitaxial Fe (solid upward triangles) [13] and Co_2MnAl (solid downward triangles) films [45], fitted with a new scaling law proposed by Tian *et al.* [13], are also given in (b). In (c), the measurements were performed at 275 K. The inset in (c) shows the electronic scattering at the surface and the interface. In (a), (b), and (c), solid lines refer to the linear fitting results.

Figure 5 shows that a_0 and b_0 (at 0 K) and the sheet resistivity ρ_{xx} at 275 K change linearly with $1/d$ for $L1_0$ FePt and FePd films, where the intercept and the slope correspond to bulk and surface contributions, respectively. It is noted that for $L1_0$ FePt and FePd, the values of b_0 fitted by the new scaling law [13], i.e., $\rho_{\mathrm{AH}}/f(T) = (\alpha + \beta\rho_{xx0})\rho_{xx0} + b_0\rho_{xx}^2$ with parameters α and β and the residual resistivity ρ_{xx0}, are close to the results of the conventional scaling law. It indicates that both a_0 and b_0 are contributed by the surface and the bulk effects, in a similar way for the longitudinal resistivity, as shown in Fig. 5(c). With larger values of a_0 and b_0 for thick samples, anomalous Hall angle, i.e., $\rho_{\mathrm{AH}}/\rho_{xx} = a_0 + b_0\rho_{xx}$, achieves larger values although the resistivity decreases with increasing d, as shown in Fig. 4. It is interesting to find the interfacial AHE *universally* exists in ferromagnetic films when the film thickness is larger than a critical value, where the longitudinal resistivity changes as a linear function of the inverse film thickness. As shown in Fig. 5(b), the parameter b of epitaxially grown Fe films, with the data taken from Ref. [13], also changes as a linear function of the inverse film thickness. Similar phenomena are also observed in b of Co_2MnAl films [in Fig. 5(b)] and Co ones [45,46]. The decrease of b_0 in thin samples may be caused by the suppression of the intrinsic AHC due to the finite-size effect [21]. Meanwhile, different electronic scattering processes in the bulk and at the surface lead to the $1/d$ linear dependence of the extrinsic side-jump term and skew scattering term. It is also interesting to find that the skew scattering term a_0 changes its sign as a function of film thickness, indicating opposite signs of contributions from the interface and the bulk. A similar sign change of a_0 is also observed in epitaxial Fe films with film thickness [13], Co/Pd multilayers with bilayer repetition [22], and $L1_0$ FePt films with annealing conditions [26]. In Co/Pd multilayers, the sign of the surface scattering induced AHE is opposite to that of the bulk one [22]. Therefore, the sign change of a_0 in $L1_0$ FePt and FePd may be caused by surface states and electron surface scattering due to the symmetry breaking, which are also influenced by different defect distribution near the surface.

The intercept, i.e., the bulk value of b_0 in $L1_0$ FePt is much larger than that of FePd. Meanwhile, the slope in b_0 of $L1_0$ FePt, corresponding to the interface contribution, is also larger than that of $L1_0$ FePd, as shown in Fig. 5(b). Similar phenomena also occur in a_0, as shown in Fig. 5(a), i.e., the bulk and the interfacial contributions to the skew scattering parameter a_0 in $L1_0$ FePt are larger than corresponding terms of $L1_0$ FePd. Therefore, the strong spin orbit interaction (SOI) effect on the interfacial AHE is clearly demonstrated. This scenario can be attributed to stronger SOI of heavier Pt atoms, compared with that of $L1_0$ FePd [25,47]. It is noted that the distribution of the density of states near the Fermi level is expected to be comparable in $L1_0$ FePt and FePd alloys with isotropic electric elements Pt and Pd and thus can be excluded in explanations of the difference in the interfacial AHE between $L1_0$ FePt and FePd. Of course, in order to fully explain the mechanism of the interfacial AHE, other factors should also be considered. Near the surface, for example, the atomic spacing of atomic layers, and thus the charge density and the electronic kinetic energy, are different from the interior ones due to the broken symmetry at the surface, which might also significantly influence the interfacial AHE. It should be noted that a_0 and b_0 quickly saturate when the film thickness is larger than 20 nm, due either to the negligible interface effect or to the tiny portion in the total AHE contributed by the interface effect, compared to the bulk effect in thicker films.

In conclusion, high-quality epitaxial $L1_0$ FePd and FePt films with different thickness d are fabricated on MgO(001) substrates and their microstructural properties are characterized by XRR at small angles and XRD at high angles. The conventional scaling law holds well for the AHE in $L1_0$ FePd and FePt films. The parameters a_0 and b_0 are found to change linearly with $1/d$ when d is smaller than 20 nm. The interface AHE is therefore clearly evidenced and is suggested to arise from the low-symmetry-induced electronic surface states and electron surface scattering in a combination with effects of different defect distribution near the surface. Furthermore, for $L1_0$ FePt films, the interface ones of either a_0 or b_0 are larger than those of $L1_0$ FePd films, and hence the SOI tuning effects of the interface AHE are demonstrated.

ACKNOWLEDGMENTS

This work was supported by the State Key Project of Fundamental Research with Grant No. 2015CB921501; the National Key Technologies R&D Program of China Grant with No. 2017YFA0303202; the National Natural Science Foundation of China (NSFC) with Grants No. 51671147, No. 11374227, No. 51331004, and No. 11774259; Shanghai Committee of Science and Technology in China (17142202300); and the Fundamental Research Funds for the Central Universities.

[1] T. Jungwirth, J. Wunderlich, and K. Olejnk, Nat. Mater. **11**, 382 (2012).
[2] A. Hoffmann, IEEE Trans. Mag. **49**, 5172 (2013).
[3] W. Zhang, W. Han, X. Jiang, S.-H. Yang, and S. S. P. Parkin, Nat. Phys. **11**, 496 (2015).
[4] L. Zhou, V. L. Grigoryan, S. Maekawa, X. Wang, and J. Xiao, Phys. Rev. B **91**, 045407 (2015).
[5] X. P. Qiu, K. Narayanapillai, Y. Wu, P. Deorani, D. Yang, W. Noh, J. Park, K. J. Lee, H. W. Lee, and H. Yang, Nat. Nano. **10**, 333 (2015).
[6] X. Zhou, M. Tang, X. L. Fan, X. P. Qiu, and S. M. Zhou, Phys. Rev. B **94**, 144427 (2016).
[7] E. H. Hall, Philos. Mag. **12**, 157 (1881).
[8] N. Nagaosa, J. Sinova, S. Onoda, A. H. MacDonald, and N. P. Ong, Rev. Mod. Phys. **82**, 1539 (2010).
[9] D. Xiao, M.-C. Chang, and Q. Niu, Rev. Mod. Phys. **82**, 1959 (2010).
[10] J. Smit, Physica (Amsterdam) **24**, 39 (1958).
[11] L. Berger, Phys. Rev. B **2**, 4559 (1970).
[12] R. Karplus and J. M. Luttinger, Phys. Rev. **95**, 1154 (1954).
[13] Y. Tian, L. Ye, and X. F. Jin, Phys. Rev. Lett. **103**, 087206 (2009).
[14] D. Yue and X. F. Jin, J. Phys. Soc. Jpn. **86**, 011006 (2015).
[15] D. Z. Hou, G. Su, Y. Tian, X. F. Jin, S. Y. A. Yang, and Q. Niu, Phys. Rev. Lett. **114**, 217203 (2015).

[16] V. L. Grigoryan, J. Xiao, X. H. Wang, and K. Xia, Phys. Rev. B **96**, 144426 (2017).
[17] L. Ye, Y. Tian, X. F. Jin, and D. Xiao, Phys. Rev. B **85**, 220403 (2012).
[18] S. L. Zhang, J. Teng, J. Y. Zhang, Y. Liu, J. W. Li, G. H. Yu, and S. G. Wang, Appl. Phys. Lett. **97**, 222504 (2010).
[19] Y. M. Lu, J. W. Cai, Z. B. Guo, and X. X. Zhang, Phys. Rev. B **87**, 094405 (2013).
[20] J. Y. Zhang, W. L. Peng, Q. Y. Sun, Y. W. Liu, B. W. Dong, X. Q. Zheng, G. H. Yu, C. Wang, Y. C. Zhao, and S. G. Wang, Appl. Surf. Sci. **436**, 22 (2018).
[21] Q. Zhang, P. Li, Y. Wen, C. Zhao, J. W. Zhang, A. Manchon, W. B. Mi, Y. Peng, and X. X. Zhang, Phys. Rev. B **94**, 024428 (2016).
[22] Z. B. Guo, W. B. Mi, R. O. Aboljadayel, B. Zhang, Q. Zhang, P. G. Barba, A. Manchon, and X. X. Zhang, Phys. Rev. B **86**, 104433 (2012).
[23] J. Y. Zhang, Z. L. Wu, S. G. Wang, C. J. Zhao, G. Yang, S. L. Zhang, Y. Liu, S. Liu, J. Teng, and G. H. Yu, Appl. Phys. Lett. **102**, 102404 (2013).
[24] K. M. Seemann, Y. Mokrousov, A. Aziz, J. Miguel, F. Kronast, W. Kuch, M. G. Blamire, A. T. Hindmarch, B. J. Hickey, I. Souza, and C. H. Marrows, Phys. Rev. Lett. **104**, 076402 (2010).
[25] P. He, L. Ma, Z. Shi, G. Y. Guo, J.-G. Zheng, Y. Xin, and S. M. Zhou, Phys. Rev. Lett. **109**, 066402 (2012).
[26] M. Chen, Z. Shi, W. J. Xu, X. X. Zhang, J. Du, and S. M. Zhou, Appl. Phys. Lett. **98**, 082503 (2011).
[27] Y. Q. Zhang, N. Y. Sun, R. Shan, J. W. Zhang, S. M. Zhou, Z. Shi, and G. Y. Guo, J. Appl. Phys. **114**, 163714 (2013).
[28] P. Czaja, F. Freimuth, J. Weischenberg, S. Blügel, and Y. Mokrousov, Phys. Rev. B **89**, 014411 (2014).
[29] J. Kudrnovský, V. Drchal, and I. Turek, Phys. Rev. B **96**, 214437 (2017).
[30] Z. Shi, H. Y. Jiang, S. M. Zhou, Y. L. Hou, Q. L. Ye, and M. S. Si, AIP Adv. **6**, 015101 (2016).
[31] B. D. Cullity, *Elements of X-Ray Diffraction* (Addison-Wesley, London, 1978).
[32] B. E. Warren, *X-Ray Diffraction* (New York, Dover, 1990).
[33] E. Yang, D. E. Laughlin, and J. G. Zhu, IEEE Trans. Magn. **48**, 7 (2012).
[34] D. A. Gilbert, L. Ye, A. Varea, S. Agramunt-Puig, N. del Valle, C. Navau, J. F. López-Barbera, K. S. Buchanan, A. Hoffmann, A. Sánchez, J. Sort, K. Liu, and J. Nogués, Nanoscale **7**, 9878 (2015).
[35] K. Y. Guslienko and A. Hoffmann, Phys. Rev. Lett. **97**, 107203 (2006).
[36] S. J. Zhang, J. G. Zheng, Z. Shi, S. M. Zhou, L. Sund, and J. Du, Thin Solid Films **520**, 5746 (2012).
[37] J. Kondo, Progr. Theoret. Phys. **32**, 37 (1964).
[38] A. Matthiessen and C. Vogt, Ann. Phys. Lpzg. **198**, 19 (1864).
[39] M. J. Otto, R. A. M. van Woerden, P. J. van der Valk, J. Wijngaard, C. F. van Bruggen, and C. Haas, J. Phys. Condens. Matter **1**, 2351 (1989).
[40] I. Mannari, Prog. Theor. Phys. **22**, 335 (1959).
[41] C. Zeng, Y. Yao, Q. Niu, and H. H. Weitering, Phys. Rev. Lett. **96**, 037204 (2006).
[42] S. Okamoto, N. Kikuchi, O. Kitakami, T. Miyazaki, Y. Shimada, and K. Fukamichi, Phys. Rev. B **66**, 024413 (2002).
[43] B. C. Sales, R. Jin, D. Mandrus, and P. Khalifah, Phys. Rev. B **73**, 224435 (2006).
[44] A. Husmann and L. J. Singh, Phys. Rev. B **73**, 172417 (2006).
[45] K. K. Meng, J. Miao, X. G. Xu, J. H. Zhao, and Y. Jiang, Phys. Lett. A **381**, 1202 (2017).
[46] J. Kötzler and W. Gil, Phys. Rev. B **72**, 060412 (2005).
[47] P. He, X. Ma, J. W. Zhang, H. B. Zhao, G. Lüpke, Z. Shi, and S. M. Zhou, Phys. Rev. Lett. **110**, 077203 (2013).